The Analysis of Tensegrity Structures for the Design of a Morphing Wing

Keith W. Moored

Hilary Bart-Smith[1]
e-mail: hb8h@virginia.edu

Department of Mechanical and Aerospace Engineering,
University of Virginia,
Charlottesville, VA, 22904

Current attempts to build fast, efficient, and maneuverable underwater vehicles have looked to nature for inspiration. However, they have all been based on traditional propulsive techniques, i.e., rotary motors. In the current study a promising and potentially revolutionary approach is taken that overcomes the limitations of these traditional methods—morphing structure concepts with integrated actuation and sensing. Inspiration for this work comes from the manta ray (Manta birostris) and other batoid fish. These creatures are highly maneuverable but are also able to cruise at high speeds over long distances. In this paper, the structural foundation for the biomimetic morphing wing is a tensegrity structure. A preliminary procedure is presented for developing morphing tensegrity structures that include actuating elements. To do this, the virtual work method has been modified to allow for individual actuation of struts and cables. The actuation response of tensegrity beams and plates are studied and results are presented. Specifically, global deflections resulting from actuation of specific elements have been calculated with or without external loads. Finally, a shape optimization analysis of different tensegrity structures to the biological displacement field will be presented.
[DOI: 10.1115/1.2424718]

Keywords: tensegrity, morphing wing, actuation, force density, biomimetics, optimization

1 Introduction

The family Myliobatidae can achieve large amplitude flapping type of locomotion and have been observed traveling at speeds greater than 1 m/s over long distances. It is these characteristics that make them attractive to study and mimic. By mimicking the movements of these species, a new underwater vehicle design is explored. The goal of this research is to develop a structure that can propel an underwater vehicle with the swift and silent motions of the manta ray. To achieve this goal, a lightweight control surface, manipulated by an active tensegrity structure, with high out-of-plane stiffness and a large range of motion under large restraining moments is being studied. Tensegrity structures are comprised of a set of discontinuous compressed struts held together with a continuous web of tensioned cables. They offer high strength to mass ratios, low mechanical wear in dynamical applications, and high deformability with minimal input energy, which makes these systems excellent candidates for the structural layout of a morphing wing. Actuation of the structure is achieved by replacing passive cables and struts with actuators. Using these structures has the potential to create a new generation of highly efficient, maneuverable air and sea vehicles. Steps towards designing and building a highly deformable and versatile morphing wing, while keeping a high enough stiffness to withstand environmental forces and perturbations, are presented.

2 Tensegrity Background

Around 1963, tensegrity structures (Fig. 1) were originally developed by Emmerich, Fuller, and Snelson, with Fuller coining the word tensegrity as a contraction of the words "tensional integrity." In recent years, tensegrity structures became of engineering interest as their potential in load bearing applications was realized, but still today these structures have not been used in many practical circumstances. To create usable structures researchers have devoted much time to the problem of form finding, which is a procedure used to determine the spatial layout of the structure.

Initial efforts by Fuller [1], Snelson [2], and Kenner [3] focused on using geometrical techniques to solve the problem of form finding. However, the internal self-stress forces of the members must be taken into account in order to have a correct theoretical model for form finding. Pellegrino [4] showed for some polyhedra that the geometric form-finding techniques were not accurate when compared to a physical model. As a result of this discrepancy several methods have been developed to accurately predict the form of a tensegrity structure. They can be categorized into two main groups: (i) kinematical methods and (ii) statical methods [5]. The *kinematical* group includes analytical, nonlinear optimization, and dynamic relaxation techniques. These methods either keep the struts lengths constant while shrinking the cables lengths or vice versa, mimicking the physical assembly of a tensegrity structure. The analytical methods give solutions for n-fold symmetric structures, i.e., prismatic tensegrities. The optimization and relaxation methods can handle generalized structures, but they become computationally intensive when asymmetries or many nodal points are involved. The *statical* techniques encompass analytical solutions, the force density method, the energy minimization method, and the reduced coordinates method. Again the analytical solutions are only viable for simple cases. The force density method, first develop by Schek [6], gives a set of linear equilibrium equations that can analyze large structures as well as asymmetric tensegrities. The energy minimization method is similar to the force density method, however the goal is to find the equilibrium configuration by finding the minimum potential energy state of the members. The reduced coordinates method is an approach that derives the equilibrium equations from the principle of virtual work, giving a model that has more control than the force density or energy minimization methods but requires more extensive calculations. Recently, Masic [7] has developed a form-finding procedure—based on the force density method—that gives

[1]Corresponding author.

Contributed by the Applied Mechanics Division of ASME for publication in the JOURNAL OF APPLIED MECHANICS. Manuscript received January 16, 2006; final manuscript received July 19, 2006. Review conducted by Robert M. McMeeking.

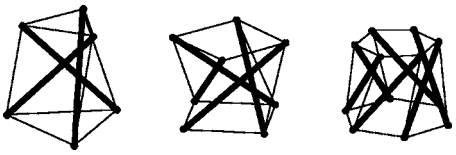

Fig. 1 Three strut, four strut, and six strut tensegrity unit cell structures

adequate control as well as quick computational times. Masic's procedure takes the force density method a step further by adding shape constraints to the structure, allowing one to manipulate the entire shape of the structure. This adapted method presents an opportunity to develop active structures, where the desired morphologies are achieved through the changes in lengths of possibly all of the members.

3 Methods

Before the tensegrity static equilibrium equations are presented some variables and operators must be defined.

DEFINITION 1. *A nodal point,* ν_k, $k=1,\ldots,n_n$, *where* n_n *is the number of nodes, is defined as a point where compressive members and tensile members connect. The vector* $\mathbf{p}=[\mathbf{x}^T,\mathbf{y}^T,\mathbf{z}^T]^T$ *is defined as the vector of nodal point locations which is decomposed into the* **x**, **y**, *and* **z** *coordinates of the nodal points, where* $\mathbf{x}\in\mathbb{R}^{nn\times 1}$, $\mathbf{y}\in\mathbb{R}^{nn\times 1}$, $\mathbf{z}\in\mathbb{R}^{nn\times 1}$, *and* $\mathbf{p}\in\mathbb{R}^{3nn\times 1}$.

DEFINITION 2. *Element* $e_i=[\nu_k,\nu_j]$, $k\neq j$, $i=1,\ldots,n_e$ *radiates from node* ν_k *and terminates at node* ν_j. *The direction of* e_i *is arbitrary, but once the direction is chosen for a given set of elements, then they must be used consistently.*

DEFINITION 3. *The cable connectivity matrix,* $\mathbf{C_{cables}}\in\mathbb{R}^{nn\times n\text{cables}}$, *is*

$$C_{\text{cables},ji}=\begin{cases}0, & \text{if } e_i \text{ does not connect to } \nu_j\\ 1, & \text{if } e_i \text{ terminates at } \nu_j\\ -1, & \text{if } e_i \text{ radiates from } \nu_j\end{cases},\quad \begin{matrix}\text{where } i=1,\ldots,n_{\text{cables}}\\ j=1,\ldots,n_n\end{matrix}$$

The strut connectivity matrix, $\mathbf{C_{struts}}\in\mathbb{R}^{nn\times n\text{struts}}$, is

$$C_{\text{struts},ji}=\begin{cases}0, & \text{if } e_i \text{ does not connect to } \nu_j\\ 1, & \text{if } e_i \text{ terminates at } \nu_j\\ -1, & \text{if } e_i \text{ radiates from } \nu_j\end{cases},\quad \begin{matrix}\text{where } i=1,\ldots,n_{\text{struts}}\\ j=1,\ldots,n_n\end{matrix}$$

The one-dimensional connectivity matrix, $\mathbf{C^1}\in\mathbb{R}^{nn\times ne}$, is

$$\mathbf{C^1}=\begin{bmatrix}-\mathbf{C_{cables}} & \mathbf{C_{struts}}\end{bmatrix} \tag{1}$$

The connectivity matrix, $\mathbf{C}\in\mathbb{R}^{3nn\times 3ne}$, is

$$\mathbf{C}=\begin{bmatrix}\mathbf{C^1} & \mathbf{0} & \mathbf{0}\\ \mathbf{0} & \mathbf{C^1} & \mathbf{0}\\ \mathbf{0} & \mathbf{0} & \mathbf{C^1}\end{bmatrix} \tag{2}$$

DEFINITION 4. *The one-dimensional force density vector,* $\lambda^1\in\mathbb{R}^{ne\times 1}$, *is*

$$\lambda_i^1=\frac{f_i}{L_i}=E_iA_i\left(\frac{1}{L_{m,i}}-\frac{1}{L_i}\right) \tag{3}$$

E is the Young's modulus; A is the area of the member; L_m is the unstressed manufacturing length of the member; and L is the final equilibrium length of the member. L is a function of nodal point positions, **p**, and is the length of a member that is in static equilibrium with the other members of the structure. The force density vector, $\lambda\in\mathbb{R}^{3ne\times 1}$, is

$$\boldsymbol{\lambda}=\begin{bmatrix}\boldsymbol{\lambda^1}\\ \boldsymbol{\lambda^1}\\ \boldsymbol{\lambda^1}\end{bmatrix} \tag{4}$$

DEFINITION 5. *The operator* (^) *is a vector operator that diagonalizes a vector*

$$\hat{\mathbf{x}}=\text{diag}([x_1,x_2,\ldots,x_n]^T)=\begin{bmatrix}x_1 & 0 & 0 & 0\\ 0 & x_2 & 0 & 0\\ 0 & 0 & \ddots & 0\\ 0 & 0 & 0 & x_n\end{bmatrix} \tag{5}$$

These definitions are similar to those presented by Masic in Ref. [7], but they differ due to the lack of member identifiers presented by Masic that describe whether a member is in compression or tension. By not having member identifiers, negative force densities are found for the compressive members and positive force densities for the tensile members. However, for the purposes of this paper the identifiers are not necessary and are therefore not presented in this formulation.

All of the statical form-finding methods for tensegrity structures find a set of equilibrium equations that are either determined by summing forces acting on a structure or using potential energy considerations. The virtual work method (VWM) uses energy considerations and the principle of virtual work to derive the equilibrium equations. The derivation is outlined in Ref. [8]. To obtain the set of equilibrium equations used in this work the virtual work method was employed. Once the set of nonlinear algebraic equilibrium equations are obtained they can be represented in a compact matrix form as the following

$$\mathbf{C}\hat{\boldsymbol{\lambda}}(\mathbf{p})\mathbf{C^T}\mathbf{p}=\mathbf{f_{ext}} \tag{6}$$

This constitutes a set of $3n_n$ unknowns, **p**, with the same number of nonlinear equations. This set of equations can be solved numerically using Matlab's *fsolve* function. Since these equations are in Cartesian coordinates, it is now simple to constrain any node to a desired value. In doing this, as can be seen from the virtual work approach, equations that are differentiated by a constrained coordinate are removed. This theoretical model gives control over all of the elements in the structure. When determining the form of a tensegrity structure using Eqs. (6), one must first set the external forces to zero to obtain the following set of equations

$$\mathbf{C}\hat{\boldsymbol{\lambda}}(\mathbf{p})\mathbf{C^T}\mathbf{p}=0 \tag{7}$$

Solving the equilibrium equations with the forces equal to zero guarantees that the structure has adequate self-stress to keep its structural integrity after the external forces have been removed.

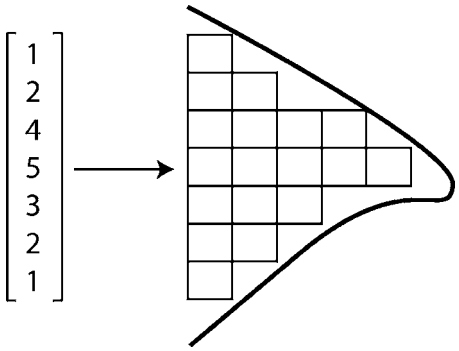

Fig. 2 The configuration vector describes the structural layout of a plate tensegrity structure composed of unit cells. Each square represents a unit cell.

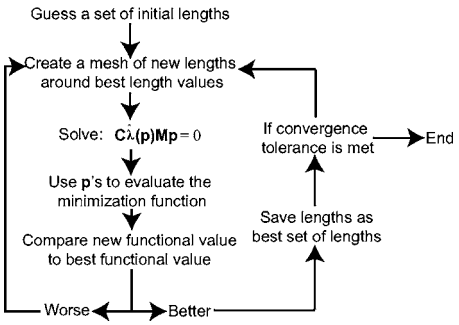

Fig. 3 Flow diagram of patternsearch optimization

For a more detailed study of the equilibrium equations and the feasibility conditions see Ref. [8].

4 Geometric Construction of a Tensegrity Plate

The initial analysis into the design of a morphing tensegrity wing examines a simple unit cell, specifically a four-strut prismatic structure (Fig. 1). Based on this system, cells are connected together to form a beam, with bar-to-bar connections between the unit cells. Instead of recreating the connectivity matrix whenever the number of cells in the beam is changed, a general connectivity matrix has been developed for any number of cells in a beam made of four-strut bar to bar tensegrities—commonly referred to as a Type 2 tensegrity structure. The generalized connectivity matrix for a Type 2 beam composed of four strut unit cells can be found in Ref. [8]. A cellular plate structure is a structure composed of many unit cells connected together that extend in two different directions. Plate structures can have many different planform shapes defined by the configuration vector (Fig. 2). If the tensegrity plate in composed of four strut unit cells with bar-to-bar connections the whole structure is considered a Type 4 structure since some nodal points have four struts connecting to them. To achieve the type of bar-to-bar connections described, the ratio of the radii of the bottom of the unit cell structure to the top of the unit cell structure must be equal to the square root of two. In order to give the structure a desired level of prestress and to solve for the initial manufacturing lengths of the symmetric unit cell, a simple force balance can be employed and is outlined in Ref. [9].

5 Actuation Mechanism

Based upon the VWM, a technique has been developed to calculate the overall topology of a tensegrity structure that has the ability to actuate strings and/or bars in an asymmetric reconfiguration. In this method, the manufacturing length becomes the actuation variable, so that, for example, a prescribed actuation strain of 20% is defined as a change in the manufacturing length of 20%. It should be pointed out that the final equilibrium length of the cable—after actuation—will not be exactly 20% different from the initial equilibrium length, due to second-order effects.

6 Optimization

The VWM is of great use in determining the global displacement field of a tensegrity structure under external loads with the actuation of individual members. By using the VWM as the foundation for the analysis, a more useful design method has been developed. Up to this point the question asked has been; what is the displacement field due to the actuation of an individual member? Instead, the question that is addressed by the following optimization routine is the inverse; which actuators are necessary to reach a given displacement field? To answer this question a direct search method known as *patternsearch* in Matlab is utilized. This method generates a mesh around an initial point, and the algorithm tests each point for a better functional value than the initial point (Fig. 3). Once a better value is achieved a mesh is generated around that point and the process repeats itself until the optimization function value has converged to a minimum. The variables for the optimization routine are the manufacturing lengths of the cables or struts, whereas the optimization function depends on the location of the nodal points.

The manta ray is the inspiration for designing a highly deformable morphing wing. However, data on the manta ray are rare since they are not easily kept in captivity. An alternative is to study the cownose ray, which is of the same family as the manta ray. The deflections of a ray's wing, as a function of time, is given in Fig. 4 [10]. Although the flapping motion of the cownose ray is asymmetric, these data present a good foundation for an optimization objective function.

The objective function is the difference between the nodal points of the top of the structure and the shape of the cownose ray's deflected wing. To obtain an equation for the shape of the cownose ray's wing an exponential curve was fit to the ray data. The following equation describes the upstroke of the ray

$$z = e^{0.1494x} - 1 \tag{8}$$

It has an R^2 value equal to 0.9901. To make this equation useful for a variety of structures of all different lengths and aspect ratios this curve must be scaled up or down compared to the length of the cownose ray's wing, which is approximately 23 cm. First a size ratio, S, comparing the spanwise length of the structure to the spanwise length of the cownose ray is defined

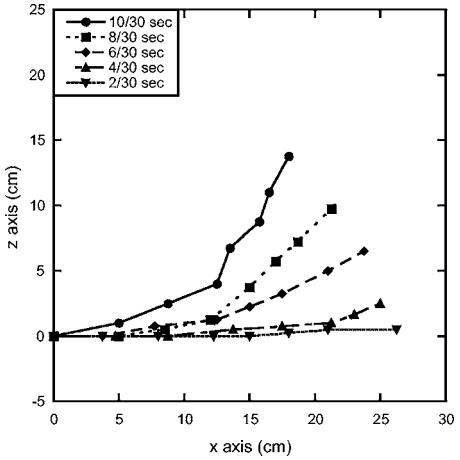

Fig. 4 Cownose ray wing curvature during a flapping cycle at different time steps. 10/30 s is the upward extreme in a normal forward propelling flapping cycle.

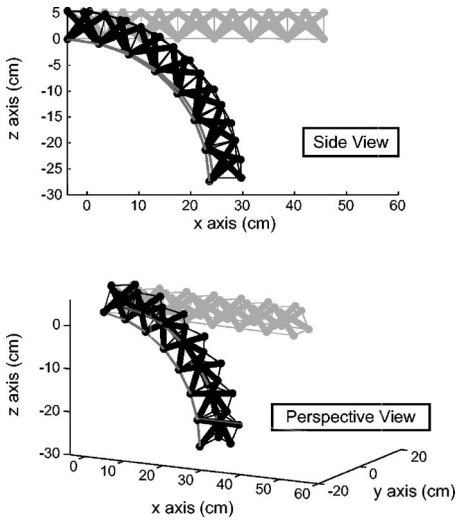

Fig. 5 61% downward deflection of a seven cell beam due to 20% contraction of the spanwise bottom cables

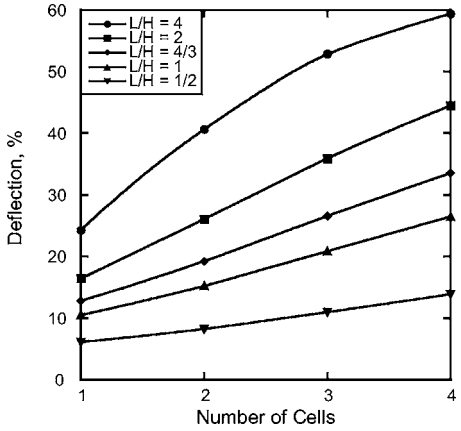

Fig. 6 Graph showing increased deflection capabilities of a beam as a function of number of cells and length to height ratio of the individual cell

$$S = \frac{L_{\text{struct}}}{L_{\text{ray}}} \tag{9}$$

A deflection ratio, D, is empirically found to be 0.6785. This ratio is measured directly from the cownose ray data. It compares the x location of the tip of the deflected wing to the x location of tip of the flat wing. This ratio gives an approximate trajectory from the flat shape to the deflected shape

$$D = \frac{x_{\text{def}}}{x_{\text{flat}}} \tag{10}$$

This allows the displacement equation to be in terms of the x locations of the initial or flat shape and not the deflected shape. By applying the S and D ratios, the curve is scaled to the size of the structure and its x values are in terms of the flat shape. Finally, the curve shifts upward to account for the initial height of the top nodes. When all of these adjustments are made to the shape equation, the following is obtained for an upstroke and downstroke, respectively

$$z = Se^{0.1494(D/S)x} - S + z_0 \tag{11}$$

$$z = -Se^{0.1494(D/S)x} + S + z_0 \tag{12}$$

Using Eqs. (11) and (12) part of the objective function is obtained. The other two parts come from the difference between the y values of the nodes and their initial y states and the x values of the top nodes and the matching deflected x values obtained from the deflection ratio. Thus the objective function is the following for a downstroke

$$\frac{1}{4}\sum_{i=1}^{n\text{top}} |x_i - Dx_{i,\text{flat}}| + \frac{1}{4}\sum_{i=1}^{n} |y_i - y_{i,0}| + \frac{1}{2}\sum_{i=1}^{n\text{top}} |z_i + Se^{0.1494(D/S)x_{i,\text{flat}}} - S_i - z_{i,0}| \tag{13}$$

The z terms of the function must be weighted more than the y terms so that the optimization does not want to converge to the initial shape—this happens because there are more y errors being computed than z errors. Also note that S is in both scalar and vector form, where the vector form is the scalar value multiplied by a ones vector, i.e., $S^*[\mathbf{1},\mathbf{1},\mathbf{1}\ldots\mathbf{1}]^{\mathbf{T}}$.

To extend the usefulness of the new optimization method, plate structures have also been studied. For a simple example a three cell by three cell plate structure has been examined. This Type 4 plate structure consisting of 132 members and 40 nodes is actuated into a twisted shape rather than a downward or upward deflection. In order to achieve a twist in the plate, the nodes on the tip of the plate are matched up to a certain degree of twist. The minimization function for the tip nodes is as follows

$$f_{\min} = \frac{1}{9}\sum_{i=1}^{n} |x_i - x_{i,0}| + \frac{4}{9}\sum_{i}^{n\text{tip}} |y_i - y_{\text{goal}}| + \frac{4}{9}\sum_{i}^{n\text{tip}} |z_i - z_{\text{goal}}|$$

$$y_{\text{goal}} = y_{i,0}\cos\theta$$

$$z_{\text{goal}} = y_{i,0}\sin\theta \tag{14}$$

where $x_{i,0}$ and $y_{i,0}$ are initial x and y nodal point positions. The summation from i to $n$tip implies summation over only the tip nodal points and the weights on each summation are somewhat arbitrary, but these values were given to reflect the relative importance of each goal. The angle θ is the prescribed or desired twist angle of the plate.

Either the deflection scenario or the twisting scenario can be cast into the following nonlinear optimization problem:

Given

$$\mathbf{p_{target}}, \mathbf{C}, \mathbf{L_m}, \mathbf{E}, \mathbf{A}, \mathbf{u_s}, \mathbf{u_c}, \mathbf{l_c}$$

$$\min_{\mathbf{L_m}} \quad f_{\min} = \sum |\mathbf{p} - \mathbf{p_{target}}|$$

such that

$$\mathbf{C}\hat{\boldsymbol{\lambda}}\mathbf{C}^{\mathbf{T}}\mathbf{p} = 0$$

$$\hat{\boldsymbol{\gamma}}\mathbf{p} = \hat{\boldsymbol{\gamma}}\mathbf{p_0}$$

$$\mathbf{L_{m,struts}} = \mathbf{u_s}$$

$$\mathbf{l_c} \le \mathbf{L_{m,cables}} \le \mathbf{u_c} \tag{15}$$

where

$$\mathbf{u_s} = \mathbf{L_{m,struts}} \quad \mathbf{l_c} = \hat{\boldsymbol{\alpha}}\mathbf{L_{m,cables}} \quad \mathbf{u_c} = \hat{\boldsymbol{\beta}}\mathbf{L_{m,cables}}$$

In this form-finding problem, γ is a vector of zeros and ones constraining certain nodal points to be fixed to their initial values; α is a vector of values between zero and one; and β is a vector of values between one and infinity. For most of the cases studied in this paper $\alpha = 0.8^*\text{ones}(n_{\text{cables}},1)$ and $\beta = 1^*\text{ones}(n_{\text{cables}},1)$. If a subset of strings is to be constrained from actuating, the α's corresponding to the subset can be set to zero that constrains the manufacturing lengths of the strings to stay at their initial values.

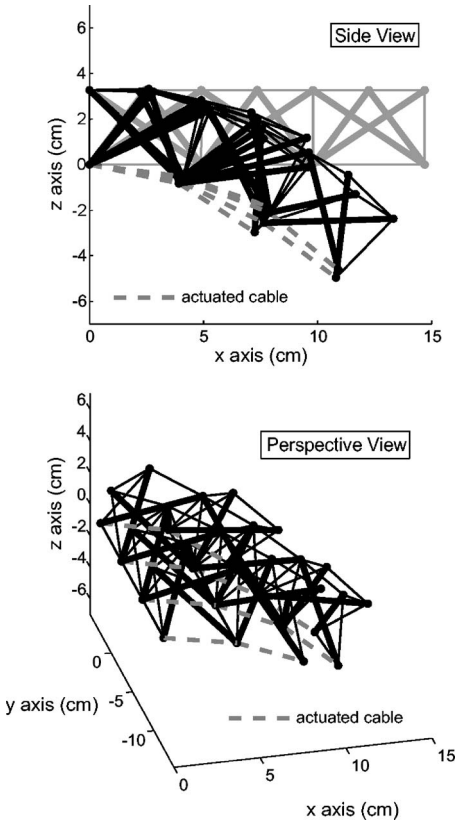

Fig. 7 34% downward deflection of a seven cell elliptical plate due to 20% contraction of the bottom spanwise cables

Results for the optimization of beams and plates to achieve deflection and twisting requirements will be presented in the following section.

7 Results

The VWM has been used to determine the global deflection of tensegrity beams and plates when individual cables are theoretically actuated. Results from the optimization scheme, developed to determine the optimal locations and contraction amounts for actuating cables, to obtain a desired displacement field, are also presented.

7.1 Beam Structures. For the multiple cell beam case, a seven cell beam was developed that consists of periodic four strut prismatic unit cells connected together bar to bar. This type of structure—based on bar-to-bar connections—is classified as a Type 2 structure. The generalized connectivity matrix was utilized to generate this beam. Three nodes are constrained at a wall such that the connected cells form a cantilever beam configuration, as shown in Fig. 5. There are no external forces acting on the structure and the bottom spanwise cables are contracted 20% each. This causes an overall downward tip deflection of 61% of the span length compared to 55% for the cownose ray, showing that this structure is capable of achieving the biological displacement field to a first-order approximation. One thing to note is that a twisting asymmetry can be seen in the final structural shape. A question that must be addressed is whether these asymmetries will be of importance in developing an actual wing. It can be seen from the seven cell beam structure that the twisting is not large, but it could have a significant effect on the fluid–structure interaction and may necessitate the need to be compensated for through additional actuation. Moreover, this asymmetry highlights the need for an op-

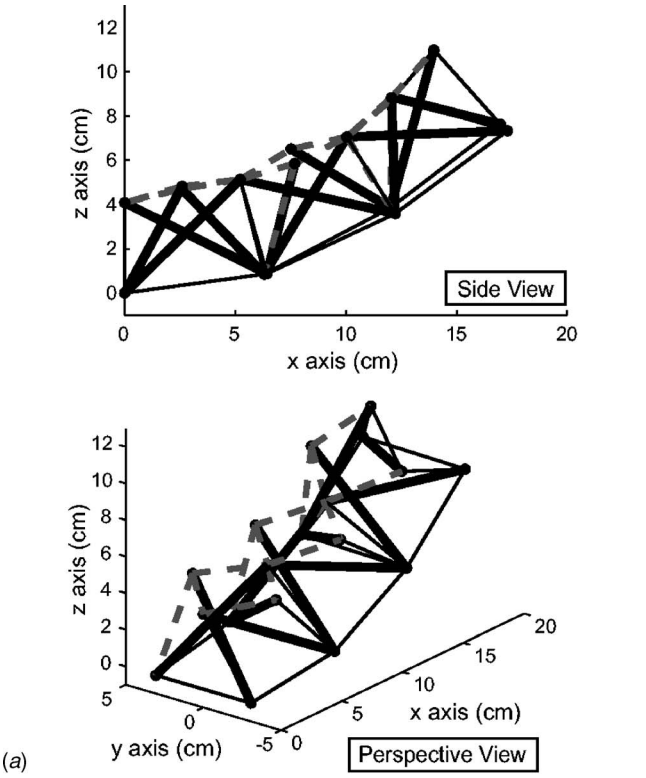

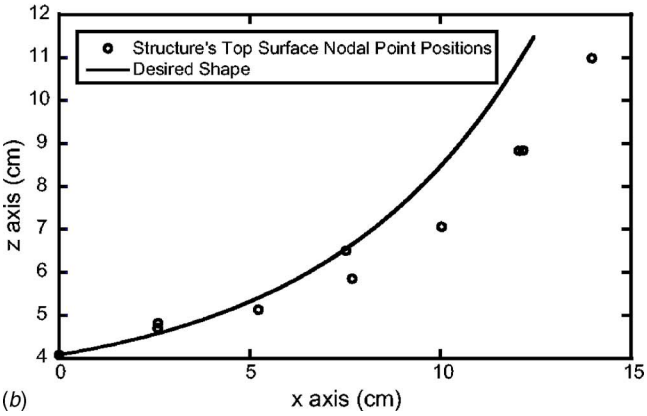

Fig. 9 (*a*) Optimal upward deflection of the unconstrained three cell beam; and (*b*) comparison of the top surface of the structure to the desired shape. With more cells or more allowed actuation strain the desired shape can be easily reached.

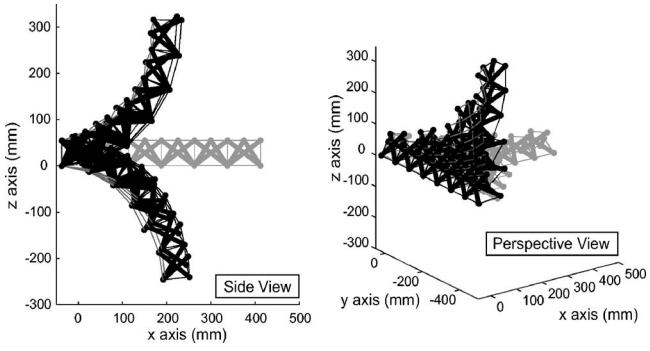

Fig. 8 63% downward and 60% upward deflection of a 19 cell manta ray shaped wing due to 20% contraction of the bottom spanwise cables and 20% contraction of the top cables, respectively

timization method that can determine which actuators to activate in order to minimize the asymmetries in the structure, while reaching the deflection goal.

Beam structures from one to seven cells in length have been studied and the tip deflection resulting from a 20% contraction of the spanwise cables have been compiled for given length to height ratios of the unit cells (Fig. 6). This shows that the addition of cells to the span will give a nonlinear increase in the maximum deflection possible for a fixed amount of contraction. Since the percent deflection is defined as the difference between the deflected tip nodal point and the initial tip nodal point the amount of percent deflection is nonlinear because the structure begins to curl in on itself. This result bodes well for future work on designing tensegrity wings, as the amount of actuation needed to achieve a given deflection decreases with increasing cells. *Deformability* is defined as the amount of tip deflection possible for a given amount of actuation. This can also be controlled by varying the amount of prestress in the structure or by varying the length to height ratio of the beam (Fig. 6).

7.2 Plate Structures. In order to create a morphing structure that has a planform resembling a ray's wing, the beam tensegrity structures must extend outward in the y direction as well as the x direction, forming a plate tensegrity structure. This structure can be thought of as a series of beam structures connected together. To construct a plate tensegrity structure, composed of individual four-strut unit cells with bar-to-bar connections, the generalized connectivity matrix for a beam structure that was previously presented can be used. However, the connections between the beams must be taken into account to construct the correct connectivity matrix. To characterize the configuration of the structure a configuration vector is prescribed, an example of which can be seen in Fig. 2. The configuration vector can be used to construct the full connectivity matrix of the plate. This is done by creating the connectivity matrix for each element of the subvector that represents a beam structure, and then compiling all of the beam connectivity matrices with the added connections between beams. The structure can then be analyzed using Eq. (7).

Two wing configurations have been studied for their actuation capabilities. The first wing configuration (Fig. 7) has an elliptical planform shape with seven four strut unit cells connected together with bar-to-bar connections, classified as a Type 4 tensegrity structure. This planform shape has a configuration vector of $[\mathbf{2}\ \mathbf{3}\ \mathbf{2}]^{\mathbf{T}}$. To determine the actuation potential of the structure, the bottom cables are contracted by the standard amount of 20% causing a 34% deflection in the–z direction.

Table 1 Errors between structural nodal points and biological data.

	Average X error (%)	Average Y error (%)	Average Z error (%)	Weighted Average error (%)
Upward unconstrained	6.26	1.11	1.06	2.11
Downward unconstrained	N/A[a]	0.75	0.29	0.4
Upward constrained	6.77	1.09	1.28	2.34
Downward constrained	N/A[a]	1.66	1.06	1.21
Designer's choice up	6.05	1.33	1.54	2.4
Designer's choice down	N/A[a]	6.65	2.47	3.52

[a]N/A=not available.

The second wing configuration (Fig. 8) has a planform shape of the cownose ray with 19 four strut cells with bar-to-bar connections, which consists of 279 members and is classified as a Type 4 tensegrity structure. This planform shape has a configuration vector of $[\mathbf{1}\ \mathbf{2}\ \mathbf{4}\ \mathbf{6}\ \mathbf{3}\ \mathbf{2}\ \mathbf{1}]^{\mathbf{T}}$. In this example the bottom cables are contracted by 20% causing a 63% downward deflection and the top cables are also actuated by 20% causing a 60% upward deflection.

The results of this analysis demonstrate the potential for these structures to mimic the kinematics of the cownose ray. However, more needs to be done to accurately mimic the biological displacement field. Moreover, if the manufacturing of one of these structures were to be made practical in terms of power consumption and cost, the structure should be designed with a minimized

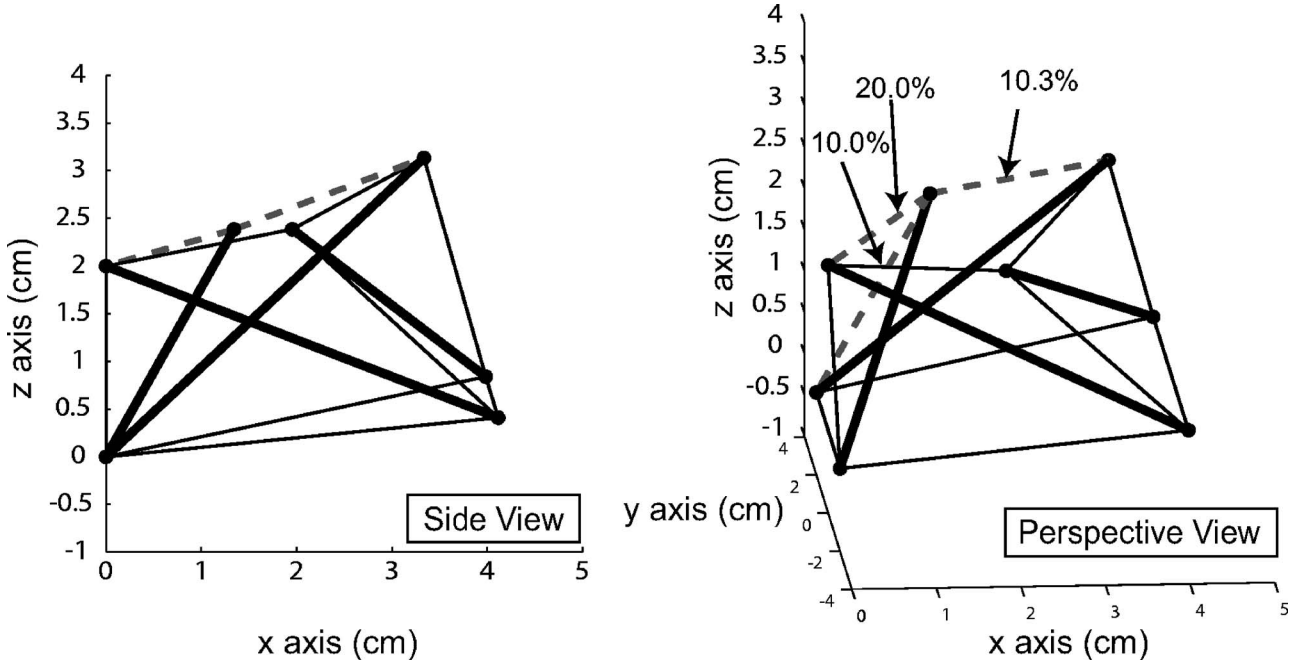

Fig. 10 Contraction amounts of individual cables in unit cell determined by the optimization scheme for upward deflection

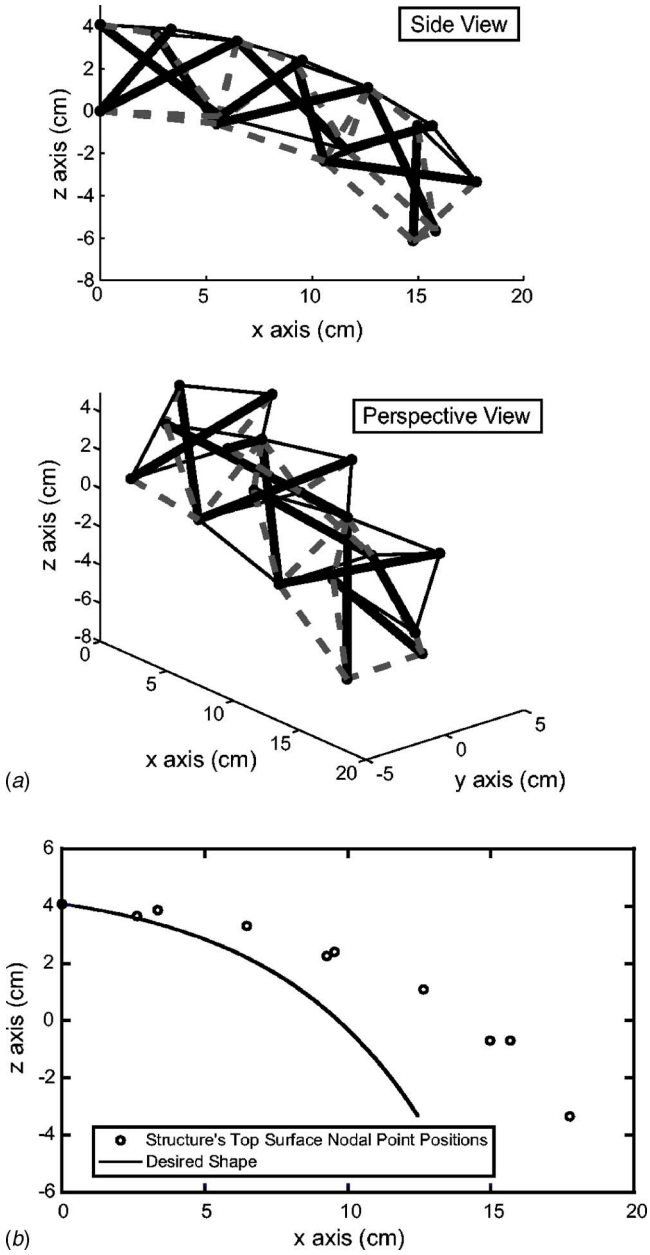

Fig. 11 (*a*) **Optimal downward deflection of the unconstrained three cell beam; and** (*b*) **comparison of the top surface of the structure to the desired shape. Since the length of the top of the structure to significantly larger than the length the cownose ray wing in a downward deflection, the structure cannot achieve the same deflection. This accounts for the large error in the *x* direction.**

number of actuation elements. To reach the biological displacement field and minimize the number of actuators, the optimization scheme described in Sec. 6 was developed.

7.3 Optimization of Deflected Beams. Using the minimization function described in Eq. (13) cantilever beams, constructed from up to four four-strut unit cells connected together, have been studied. The unit cells are connected bar-to-bar forming a Type 2 tensegrity structure. The maximum allowed contraction percentage is set to 20% of the manufacturing lengths of specified members. This new optimization design tool determines which actuating cables are required to contract and by how much, in order to reach a desired shape or displacement field, subject to predefined constraints. Four distinct cases have been studied. The minimization function for the four optimization cases is strongly weighted to ensure the smallest error occurs for the vertical deflections. As the number of cells in the beam is increased, the structure's ability to achieve and resolve the desired shape strengthens—i.e., the errors get smaller as the number of cells increase. This is an expected consequence as the number of degrees of freedom also increases, allowing for finer shape changes.

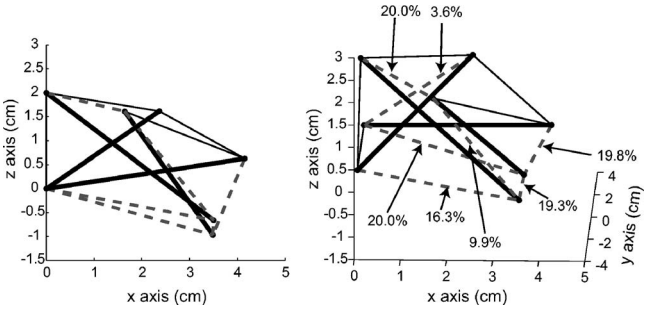

Fig. 12 Contraction amounts of individual cables in unit cell determined by the optimization scheme for downward deflection

The first shape optimization case is an upward deflection where the top nodal points of a structure are matched to the cownose deflected shape and the design space is unconstrained, meaning that all of the cables are possible actuators. The unconstrained problem reaches small minimization functional values, i.e., with all cables being potential actuators; the shape of the structure will be close to the desired shape. The actuation results for a three cell cantilever beam can be seen in Fig. 9. The unconstrained case gives excellent agreement to the cownose data with only three cells connected together with the errors falling to less than 2% in the z direction (Table 1). The greatest source of error is in the x direction which can be reduced by allowing for larger actuation strains than 20% or by increasing the amount of cells in the spanwise direction. An example of the contraction percentages of the cables for the unconstrained case of a single cell beam are given in Fig. 10, for an upward deflection.

For the second case study, the deflected shape of the top nodes of the structure is optimized to achieve the downward deflected shape of the cownose ray, given an unconstrained design space. Figure 11 shows the deflected shape of a three cell beam. The unconstrained problem produces some interesting results in terms of which cables are actuated. As can be seen in Fig. 11, several of the cables connecting the top and bottom layers of the structure are actuated. This is to be expected due to the fact that it is the top surface of the structure that is being matched to the downward deflection field. Again, there is excellent agreement in the unconstrained case with the cownose data (Table 1), except in the x direction. As an example of the contraction percentages the unconstrained case is shown for a single cell beam in Fig. 12, performing a downward deflection.

The x direction error is listed in Table 1 as not applicable because the error between the desired shape and the structural shape cannot be compared in the x direction. This inconsistency arises because the top surface of the structure is matched to the desired shape, while the structure is deflecting downward. In this situation the length of the desired shape curve is significantly shorter than the length of the top surface of the structure leading to a situation where the structure can never reach the desired shape. Since the z direction is the preferential direction in the minimization function the optimization obtains results where the z direction error was very small and the x direction error was very large. If one where to prescribe the x direction as the preferential direction the optimization would obtain results with a small x direction error and a large z direction error. One way to achieve small errors in both the x and z directions would be to scale up the size of the desired shape, however this is not consistent with the cownose ray data

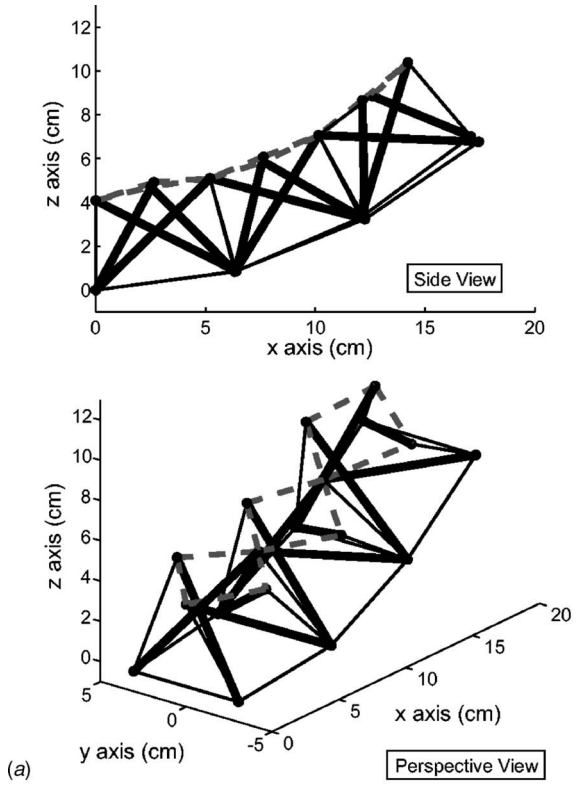

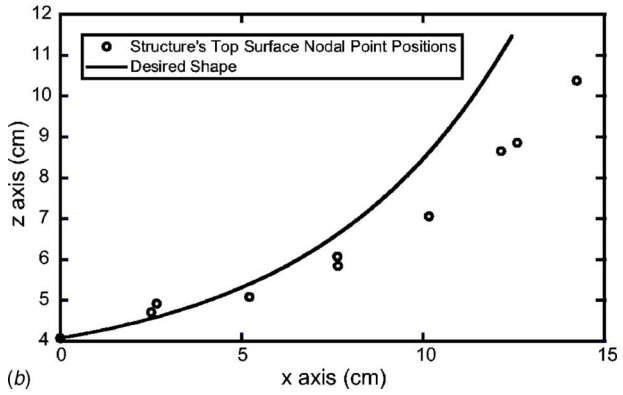

Fig. 13 (*a*) **Optimal upward deflection of the constrained three cell beam; and** (*b*) **comparison of the top surface of the structure to the desired shape**

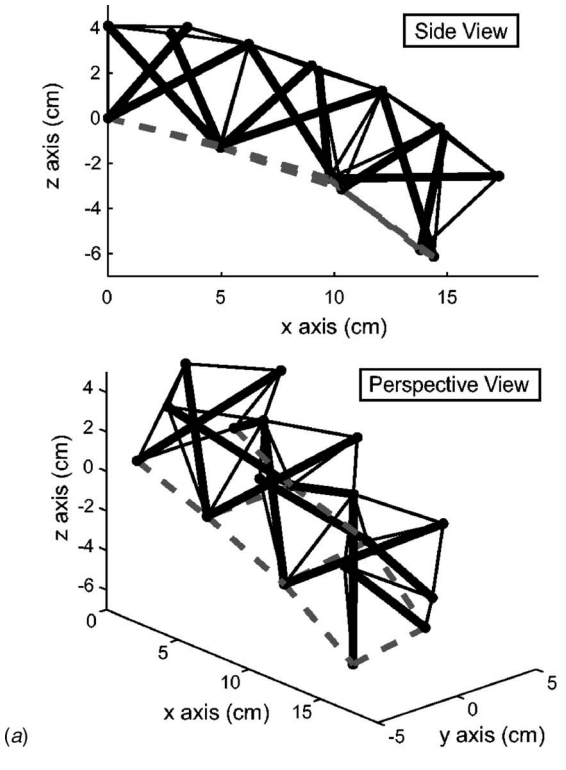

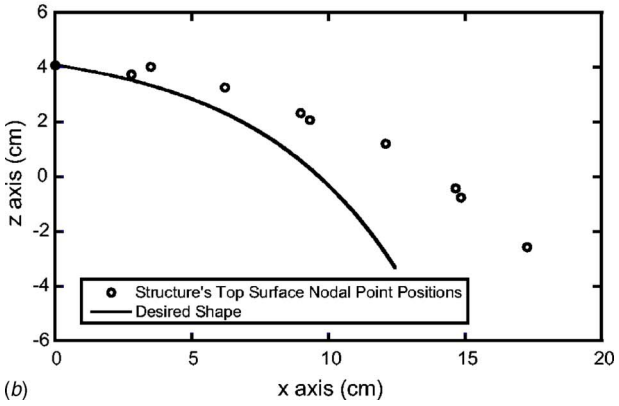

Fig. 14 (*a*) **Optimal downward deflection of the constrained three cell beam; and** (*b*) **comparison of the top surface of the structure to the desired shape**

set. The best way to achieve small error in both directions is to match the bottom surface of the structure to the desired shape in a downward deflection. This relieves the structure of the physical constraint presented in the top surface optimization for a downward deflection.

From the first and second cases the unconstrained problem is shown to be an excellent starting point for determining which sets of actuators are the dominant actuators for a given shape change and even in some cases the unconstrained design space may prove feasible in terms of manufacturability. However, the unconstrained problem typically is not practical since the optimization produces a structure with a large number of active members, making it difficult to build and more expensive to operate. But a constrained optimization case can be used that limits the potential actuators to a certain subset of the members, i.e., the dominant active members from the unconstrained case. The third and fourth cases explore the constrained problem for the upward and downward deflections.

The third shape optimization case is an upward deflection where the top nodal points of the structure are matched to the cownose deflected shape and the design space is constrained to the top cables as potential actuators. The actuation results for a three cell cantilever beam can be seen in Fig. 13. For the constrained case the error between the desired shape and the optimized shape increases slightly over the unconstrained problem, but still gives very good agreement with the biological data (Table 1).

The fourth case studied optimizes the deflected shape of the top nodes of the structure to the downward deflected shape of the cownose ray with a potential actuator space constrained to only the bottom cables. Figure 14 shows the deflected shape of a three cell beam. There is excellent agreement in the constrained case with the cownose data (Table 1) and the errors are only slightly higher than the unconstrained case.

Both the unconstrained and the constrained cases reach much closer to the actual cownose shape than a designer's choice of the actuator locations and amounts (Table 1). In order to evaluate the overall performance of all design choices a weighted average error has been calculated. This error takes into account the weights of the minimization function, which gives the z direction the

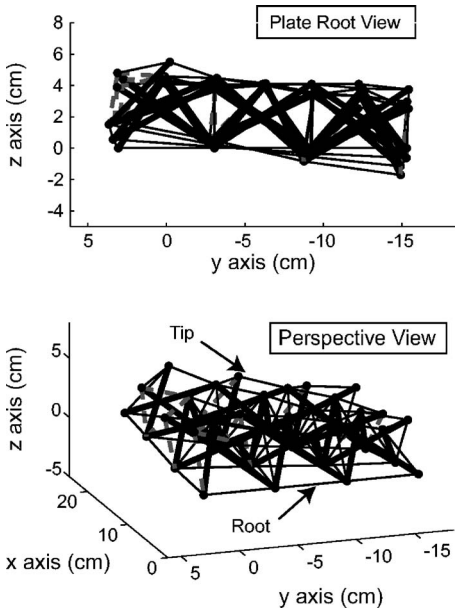

Fig. 15 Nine cell plate optimized for a 15 deg twist

strongest influence. Table 1 highlights the two main reasons for using this optimization method as a design tool: (1) when designing a tensegrity structure to reach a specific shape it is not intuitive which members should be actuators and (2) when the active members are chosen it is not intuitive by how much they should be actuated.

7.4 Optimization of a Twisting Plate. The minimization function presented in Eq. (14) is used to optimize the end nodes of a three cell by three cell plate structure to achieve a prescribed twist angle of 15 deg. The results of this optimization are shown in Fig. 15. The dotted lines represent the active cables, the solid thin lines are the passive cables and the solid thick lines are the struts. The average errors in the x, y, and z directions are 0.67%, 1.36%, and 1.46%, giving an excellent agreement with the desired shape. This example has shown the robustness of the optimization design tool developed in this paper. The method can handle any structural compositions as well as any desired shape by determining a new minimization function for each shape. Material property constraints may also be added once the materials are chosen.

8 Conclusions

This paper applies the virtual work method to the problem of form finding of tensegrity structures. By actuating individual elements using the virtual work method, deformation of single and multiple cell beams were studied. A new optimization design tool was presented which can determine which elements in a structure need to be actuated and by how much in order to reach a desired shape. In particular it was shown that a tensegrity beam structure can match very closely to the biological displacement of the cownose ray with only a few cells connected together. The optimization tool is a necessary step in the design of a morphing wing when the shape of the activated wing must be close to a desired displacement field. As the desired displacement field becomes more complex this optimization method becomes more important. However, any intuitive approach can be improved upon by using this design tool.

Acknowledgment

Keith William Moored and Hilary Bart-Smith gratefully acknowledge the support of the National Science Foundation through Award No. 0348448 and the David and Lucille Packard Foundation through the Packard Fellowship for Science and Engineering.

Nomenclature

$\mathbf{p}$ = nodal point vector
$\mathbf{x}$ = x coordinate vector of nodal points
$\mathbf{y}$ = y coordinate vector of nodal points
$\mathbf{z}$ = z coordinate vector of nodal points
$\mathbf{x_0}$ = initial x positions
$\mathbf{y_0}$ = initial y positions
$\mathbf{z_0}$ = initial z positions
$\mathbf{f}_{\text{ext}}$ = external force at a node
λ = force density in a member
$\boldsymbol{\lambda}^{\mathbf{1}}$ = one-dimensional force density vector
$\boldsymbol{\lambda}$ = three-dimensional force density vector
f = internal force in a member
L = equilibrium length
L_m = unstressed manufacturing length
E = Young's modulus
A = cross-sectional area
n_n = number of nodes
n_e = number of elements
$\mathbf{C}^{\mathbf{1}}$ = one dimensional connectivity matrix
$\mathbf{C}$ = three-dimensional connectivity matrix
$\mathbf{C_{cables}}$ = full cable connectivity matrix
$\mathbf{C_{struts}}$ = full strut connectivity matrix
L_{struct} = characteristic length of the structure
L_{ray} = characteristic length of the cownose ray wing
S = size ratio
D = deflection ratio
x_{def} = deflected x coordinates of a structure
x_{flat} = flat x coordinate of a structure
n_{top} = number of top nodes
n_{tip} = number of tip nodes
f_{min} = minimization function
θ = desired angle of twist
$\mathbf{p_{target}}$ = desired nodal point positions
$\mathbf{u_s}$ = upper bound of the struts
$\mathbf{u_c}$ = upper bound of the cables
$\mathbf{l_c}$ = lower bound of the cables
$\boldsymbol{\gamma}$ = constraint parameter
$\boldsymbol{\alpha}$ = cable lower bound parameter
$\boldsymbol{\beta}$ = cable upper bound parameter

References

[1] Fuller, R. B., 1962, *Tensile-Integrity Structures*, U.S. Patent and Trademark Office, Washington, D.C.
[2] Snelson, K. D., 1965, *Continuous Tension, Discontinuous Compression Structures*, U.S. Patent and Trademark Office, Washington, D.C.
[3] Kenner, H., 1976, *Geodesic Math and How to Use It*, University of California Press, Berkley, CA.
[4] Pellegrino, S., 1986, *Mechanics of Kinematically Indeterminate Structures*, University of Cambridge Press, Cambridge, UK
[5] Tibert, A. G., and Pellegrino, S., 2003, "Review of Form-Finding Methods for Tensegrity Structures," Int. J. Space Struct., **18**(4), pp. 209–223.
[6] Schek, H. J., 1974, "The Force Density Method for Form Finding and Computation of General Networks," Comput. Methods Appl. Mech. Eng., **3**, pp. 115–134.
[7] Masic, M., Skelton, R. E., and Gill, P. E., 2005, "Algebraic Tensegrity Form-Finding," Int. J. Solids Struct., **42**(16–17), pp. 4833–4858.
[8] Moored, K. W., and Bart-Smith, H., 2005, "The Analysis of Tensegrity Structures for the Design of a Morphing Wing," *Proceedings of IMECE'05*, Orlando, FL, November 8–12, ASME, New York.
[9] Masic, M., and Skelton, R., 2004, "Open Loop Control of Class-2 Tensegrity Towers," Proceedings SPIE's 11th Annual International Symposium on Smart Structures and Materials. San Diego, CA.
[10] Heine, C., 1992, *Mechanics of Flapping Fin Locomotion in the Cownose Ray, Rhinoptera Bonasus (Elasmobranchii, Myliobatidae)*, Duke University Press, Durham, NC.